Petroleum Science 19 (2022) 861–869

Contents lists available at ScienceDirect

Petroleum Science

journal homepage: www.keaipublishing.com/en/journals/petroleum-science

Original Paper

$Ce_2(MoO_4)_3$ as an efficient catalyst for aerobic oxidative desulfurization of fuels

Xiao-Yi Liu, Xiu-Ping Li, Rong-Xiang Zhao*

School of Petrochemical Engineering, Liaoning Petrochemical University, Fushun, 113001, Liaoning, China

ARTICLE INFO

Article history:
Received 9 June 2021
Accepted 28 October 2021
Available online 13 January 2022

Edited by Xiu-Qiu Peng

Keywords:
$Ce_2(MoO_4)_3$
Aerobic oxidative desulfurization
Dibenzothiophene
Reflux
Renewability

ABSTRACT

$Ce_2(MoO_4)_3$ was synthesized by a simple reflux method using cerium nitrate hexahydrate and ammonium molybdate as reactants. The as-prepared $Ce_2(MoO_4)_3$ was characterized by Fourier transform infrared spectroscopy (FT-IR), X-ray diffraction (XRD), Scanning electron microscope (SEM), and X-ray photoelectron spectroscopy (XPS). The removal of dibenzothiophene (DBT) in model oil was studied using $Ce_2(MoO_4)_3$ as catalyst and oxygen as oxidant. The reaction factors such as reaction temperature, amount of catalyst, and sulfide type on sulfur removal were researched. The results prove that both Ce^{3+} and MoO_4^{2-} play significant role in the conversion from DBT to $DBTO_2$. The $Ce_2(MoO_4)_3$ catalyst has an excellent performance for the sulfur removal of DBT. Under the optimum reaction conditions, sulfur removal of 99.6% was obtained. After recycling five times, no significant loss in catalyst activity of $Ce_2(MoO_4)_3$. Mechanism of aerobic oxidative desulfurization was proposed based on the experiment of free radical capture and infrared characterization.

1. Introduction

The emission of sulfur oxides (SO_X) in vehicle exhaust can cause serious environmental problems and threaten human health. Thus, countries around the world have set up strict limits on the sulfide content in fuels, and it is very urgent to develop efficient deep desulfurization technology. In recent years, hydrodesulfurization (HDS) has been widely used to remove organic sulfur compounds, which is conducted at harsh reaction conditions (300–350 °C, 2–10 MPa) with expensive hydrogenation catalysts. HDS can effectively remove aliphatic sulfur compounds (Sampieri et al., 2005). Furthermore, removal of aromatic sulfur compounds is difficult because steric hindrance. Some technologies have been developed to overcoming technical defects of HDS, these desulfurization technologies are adsorption desulfurization (ADS) (Luo et al., 2021), extractive desulfurization (EDS) (Li et al., 2013) and oxidative desulfurization (ODS) (Wang et al., 2018), etc. Among them, the ODS technology has been widely researched due to its advantages such as mild operating conditions, low energy consumption, and high removal efficiency of aromatic sulfides. In the ODS process, organic sulfides can be oxidized into sulfones with strong polarity, and then removed by extraction or adsorption (Zhen et al., 2019). Various oxidants, including H_2O_2, oxygen and organic peroxides have been applied to the ODS process. H_2O_2 is widely used due to its lower cost, higher oxidation performance and environmental protection. However, the production and storage of hydrogen peroxide may cause safety and cost issues (Liu et al., 2021). Oxygen is not only environmentally friendly, moreover it is easy to get. Thus, oxygen as the oxidant in ODS, it has attracted the attention of researchers (Wang et al., 2021).

In ODS, the reaction between oxygen and sulfide is difficult to be carried out under mild conditions. Therefore, it is very important to develop high activity catalysts. In recent years, some catalysts, such as inert metal-based material (Nakagawa et al., 2019), metal organic frameworks (MOFs) (Tang et al., 2020), polyoxometalate (POMs) (Chi et al., 2019), transition metal oxide (TMO) (Wang et al., 2017) etc., are applied to the field of aerobic oxidative desulfurization (AODS). TMO has been widely concerned in ODS due to their higher activity and lower cost (Wang et al., 2020). For example, Wang et al. (Wang et al., 2020) synthesized V_2O_5 nanosheets with oxygen vacancies by rapid gas drive stripping method. The sulfur removal can reach 99.7% under the optimum reaction conditions. Shi et al., (2016) proposed a simple sol-gel method to prepare Ce–Mo–O catalysts. The catalyst can completely remove BT and 4, 6-DMDBT, the removal rate of BT is

* Corresponding author.
E-mail address: Liuxiaoyi1029@126.com (R.-X. Zhao).

https://doi.org/10.1016/j.petsci.2021.10.029

List of symbols

C_0	Sulfur compound contents before reaction, μg/g
C_t	Sulfur compound contents at reaction time t, μg/g

Greek letters

η	Sulfur removal, %

97%, and the oxidation process does not need to add sacrificial agent. Dong (Dong et al., 2019) et al. has developed ultra-thin a-$CO(OH)_2$ nanosheets with molybdate intercalation, its derived Co–Mo–O mixed metal oxide has shown excellent sulfur removal performance. Wu et al., (2020) found that the interaction of strong metal edges between Pt and h-BN can improve the aerobic oxygen oxidation performance in fuel oil. Liu et al., (2020) established Co–Ni–Mo–O mixed metal oxide nanotubes with a hollow structure preferred to application of AODS. The preparation of the above catalysts often requires harsh preparation conditions such as calcination or the addition of organic reagents to control the structure of the catalyst. These defects are not conducive to the industrialization process of aerobic oxidative desulfurization.

Cerium molybdate has been widely applied in the fields of inorganic pigments (Dargahi et al., 2020) and photocatalysts (Xing et al., 2016). At present, there is no report of cerium molybdate used as a catalyst for AODS. In this paper, $Ce_2(MoO_4)_3$ was synthesized and characterized by FT-IR, XRD, SEM, XPS. Compared with the previous TMO, the synthesis of the $Ce_2(MoO_4)_3$ can be carried out under mild reaction conditions (lower temperature and shorter reaction time), and the reaction process does not need to add structure promoter and high-temperature calcination. The oxidative desulfurization of model oil was determined by using $Ce_2(MoO_4)_3$ as the catalyst and oxygen as the oxidant. Furthermore, based on the experimental conclusion, the functions of Ce and MoO_4 are illustrated in ODS, and proposed possible reaction mechanism.

2. Experimental

2.1. Materials and instruments

Ammonium molybdate (98 wt%), Cerium Nitrate Hexahydrate (AR), Decahydronaphthalene (AR), Dibenzothiophene (AR), 4,6-Dimethyldibenzothiophene (AR), Benzothiophene (AR), All above reagents were purchased from Aladdin Reagent Co., Ltd.. Oxygen (99 wt%, Hubei Guangao Biological Technology Co., Ltd.).

FT-IR of the synthesized catalysts was characterized by a Nicolet FT-IR spectrophotometer (Nexus 470, Thermo Electron Corporation) with spectral range of 4000-400cm-1 and resolution better than 1.5 cm^{-1}. XRD graphics of the $Ce_2(MoO_4)_3$ sample were obtained using the Philips diffractometer utilizing high-intensity Cu Kα radiation in X'Pert MPD model (40 kV; 100 mA; 1.5406 Å), and the step scan technique at 2 theta angles range between 10° and 70°. Surface morphology of the $Ce_2(MoO_4)_3$ was characterized by SEM (ZEISS Gemini SEM 500, Germany). The elemental composition of the $Ce_2(MoO_4)_3$ was studied by energy-dispersive X-ray spectroscopy (EDS). XPS (PHI5000 Versaprobe II, Japan) was used to survey and evaluate the elemental composition and surface chemical state of $Ce_2(MoO_4)_3$.

2.2. Synthesis of $Ce_2(MoO_4)_3$

In this work, the $Ce_2(MoO_4)_3$ catalyst was synthesized by the reflux method. 0.5296g ammonium molybdate was dissolved in 40 mL distilled water, marked as solution-A, then, solution-A was added to a triangular flask with a cooling condenser. After that, aqueous solution (40 mL) of 0.8744g cerium nitrate hexahydrate was added dropwise to Solution-A. The triangular flask containing the mixed solution was transferred to an oil bath and stirred at 80 °C for 1 h. The pale yellow precipitation was obtained. The products after centrifugal separation were washed three times with absolute ethanol and distilled water, and dried at 90 °C for 5 h.

2.3. Aerobic oxidation desulfurization experiments

The model oil with S-content of 250 μg/g was prepared by dissolving 0.718g dibenzothiophene in 500 mL decahydronaphthalene. The AODS reaction was carried out in a three-neck flask. Firstly, 20 mL simulated oil and a certain amount of $Ce_2(MoO_4)_3$ were added to three-necked flask with reflux device. Then, the three-neck flask was placed in a preheated oil bath. oxygen was injected at a flow rate of 0.2L/min. The AODS reaction begins at a certain temperature and agitation speed. A small amount of upper oil phase is taken as sample every 20 min and the sulfur content of the sample was measured by WK-2D microcoulomb analyzer, then calculation of sulfur removal by formula (1). The reaction device is shown in Fig. 1.

$$\eta = \left(\frac{C_0 - C_t}{C_0}\right) \times 100\% \quad (1)$$

3. Results and discussion

3.1. Characterization

3.1.1. FT-IR and XRD analysis

The FT-IR and XRD characterization results of the as-synthesized $Ce_2(MoO_4)_3$ are revealed in Fig. 2. As shown in Fig. 2(a), the infrared absorption peaks at 3382 cm^{-1} and 1616 cm^{-1} are attributed to stretching and bending mode of O–H from water adsorbed on the surface of samples (Xing et al., 2016), the smaller peak at 1384 cm^{-1} corresponds to the bending vibration of the Ce–O–H bond. The

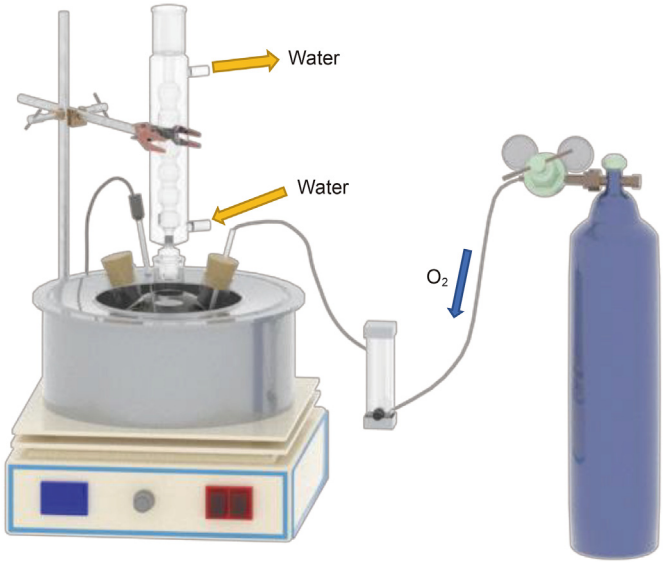

Fig. 1. Device diagram of aerobic oxidative desulfurization.

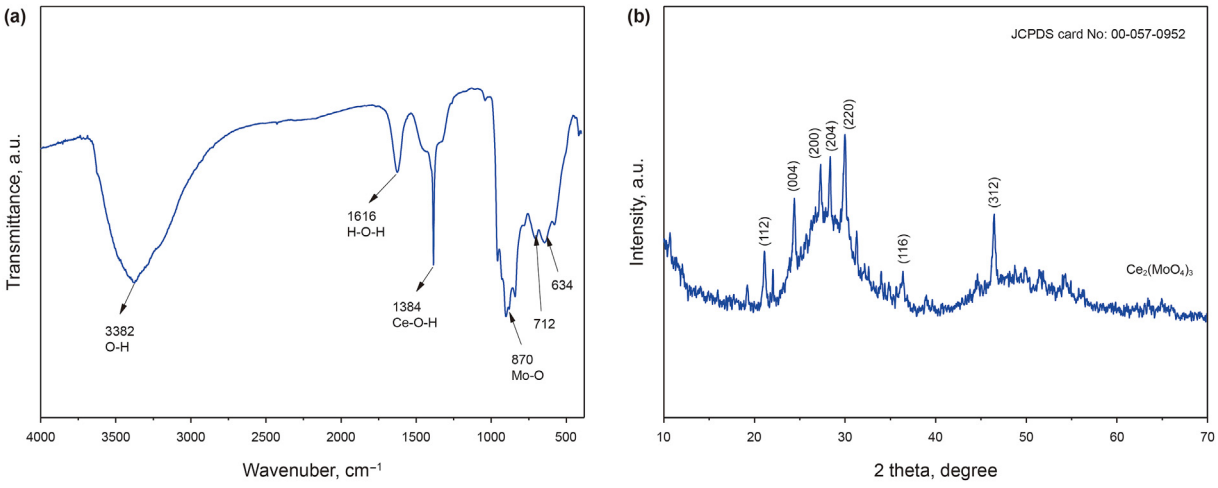

Fig. 2. **(a)** FT-IR and **(b)** XRD spectra of $Ce_2(MoO_4)_3$.

narrow peaks between 1070 and 1150 cm^{-1}, the peaks around 870, 712 and 634 cm^{-1} associate to the stretching vibration peaks of the Mo—O bond (Yousefi et al., 2012). Crystallinity of $Ce_2(MoO_4)_3$ was determined by XRD analysis. The XRD patterns are shown in Fig. 2(b). From the results, typical characteristic peaks of samples associate to $Ce_2(MoO_4)_3$ crystals (JCPDS: 00-057-0952) and the structure is amorphous nanocrystal (Kartsonakis and Kordas, 2010). The individual peaks at 2θ angles are obtained to 21.19°, 24.47°, 27.61°, 28.33°, 29.99°, 36.39°and 46.34°, which are assigned to (112), (004), (200), (204), (220), (116), (312) planes of monoclinic $Ce_2(MoO_4)_3$, respectively. No peak of other crystal phases is observed in the spectrum.

3.1.2. SEM analysis

The morphology of the as-prepared $Ce_2(MoO_4)_3$ was investigated by SEM. As shown in Fig. 3(a), the sample is composed of nanocrystals with rod-like structure and particles. The particle size of nanocrystals is uneven due to lower reaction temperature and shorter reaction time. Moreover, nanocrystals were revealed high dispersibility and low packing density. According to relevant reports (Xing et al., 2016), the morphology of $Ce_2(MoO_4)_3$ can be changed according to different synthesis conditions. The EDS measurement of the sample is shown in Fig. 3 (b), indicates that the sample is composed of Ce, Mo and O elements, and its molar ratio is approximately n(Ce): n(Mo): n(O) = 2:3:12. It is consistent with the composition of cerium molybdate.

3.1.3. XPS analysis

For the benefit of obtaining the composition and chemical state of catalyst, XPS analysis of $Ce_2(MoO_4)_3$ catalysts was performed. As shown in Fig. 4(a), the survey curves of catalysts further demonstrate the coexistence of Ce, Mo and O elements, each element has a spin-orbit core energy level. Among them, the spin-orbit energy spectrum of Ce elements can be divided into two multiple energy levels (U and V), they correspond to the core-level spin-orbit splitting of Ce $3d_{3/2}$ and Ce $3d_{5/2}$ (Kanai et al., 2017). The high-resolution XPS spectrum of Ce 3d was shown in Fig. 4(b), the U_0, V_0, U_1, V_1 peaks corresponding to Ce^{3+} state and the remaining 5 peaks corresponding to Ce^{4+} state (Sakthivel et al., 2015). The presence of Ce^{3+} and Ce^{4+} indicates that the $Ce_2(MoO_4)_3$ catalyst has redox properties.

The high-resolution XPS spectrum of the spin-orbit core energy level of O1s was displayed Fig. 4(c). The sharp peak observed at 530.51 eV assigned to lattice oxygen in the Mo—O bond. And the

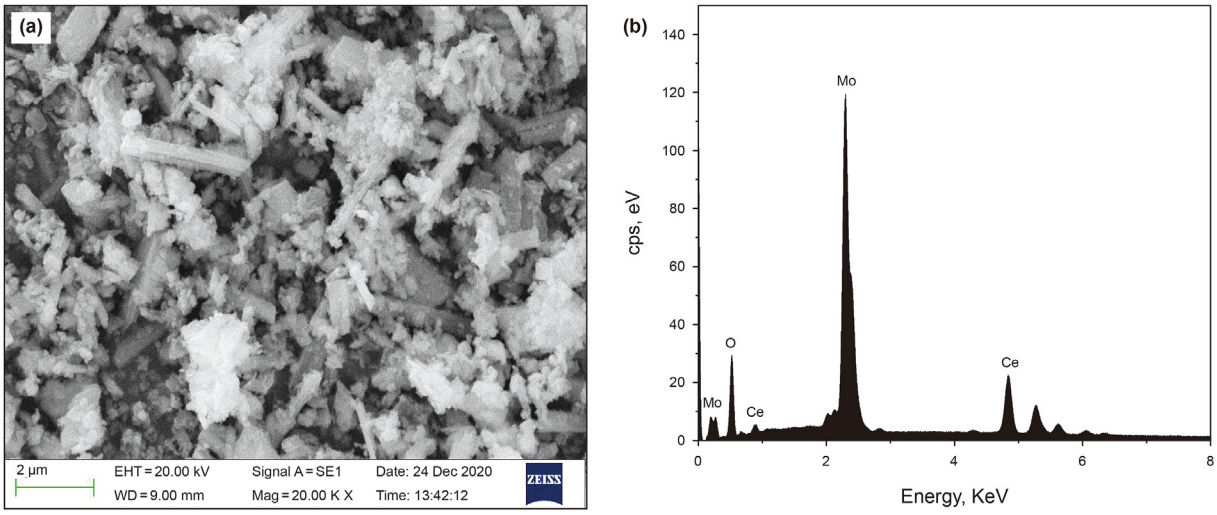

Fig. 3. **(a)** SEM and **(b)** EDS images of $Ce_2(MoO_4)_3$.

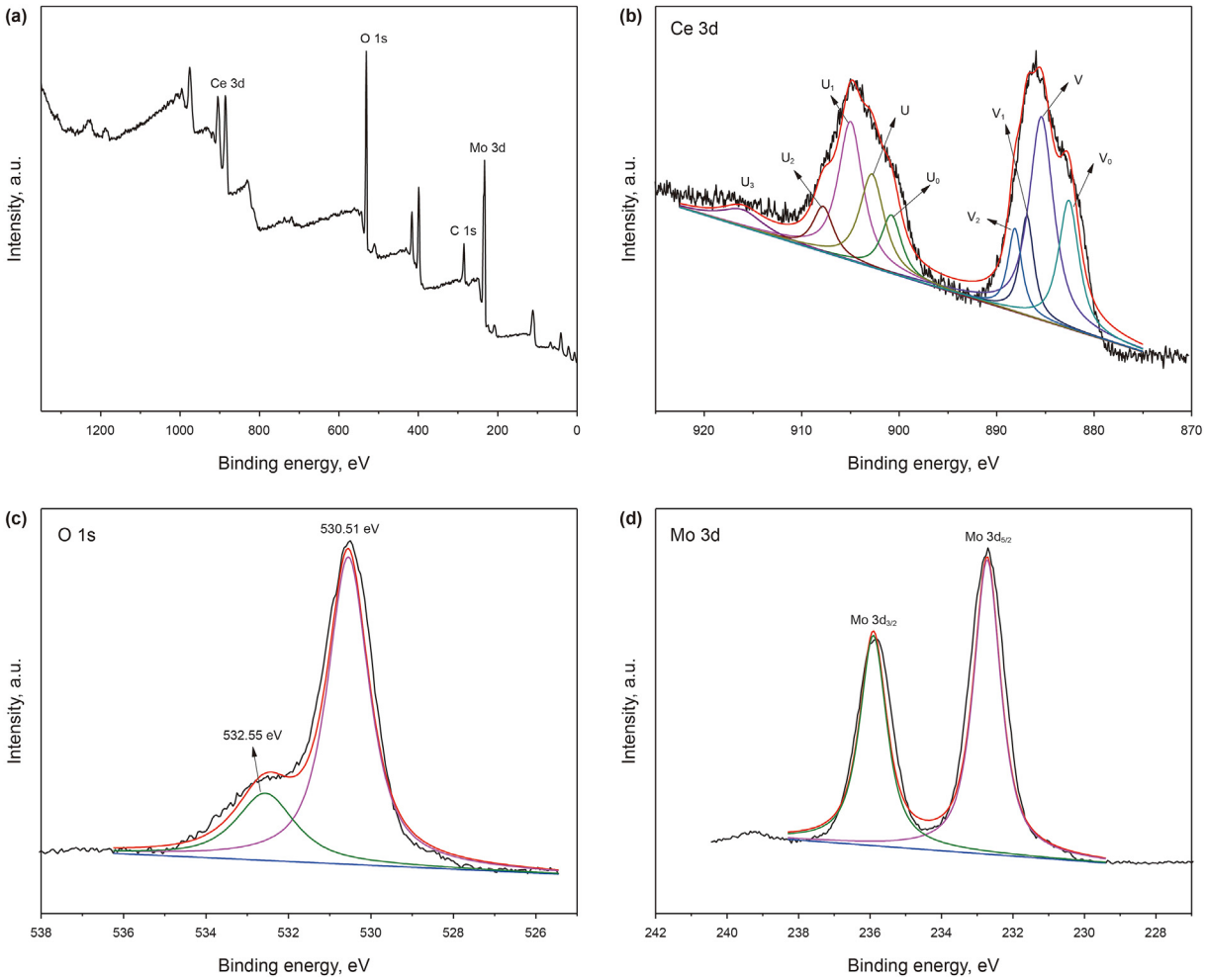

Fig. 4. XPS spectrum of **(a)** $Ce_2(MoO_4)_3$, high resolution spectra of **(b)** Ce3d, **(c)** O1s and **(d)** Mo3d.

side peak at 532.55 eV can be corresponded the O_2 was adsorbed on $Ce_2(MoO_4)_3$ surface (Sakthivel et al., 2015).

The XPS spectrum of the spin-orbit core energy levels of Mo $3d_{5/2}$ and Mo $3d_{3/2}$, the binding energy at 232.68 eV related to the Mo^{6+} oxidation state of the Mo $3d_{5/2}$ spin-orbit core energy level in Fig. 4 (d). The other peak appears at 235.87 eV is the Mo $3d_{3/2}$ spin-orbit core energy level of Mo^{6+} oxidation state, it can be attributed to the existence of Mo=O or Mo—O bond, but no additional peaks of Mo^{4+} or Mo^{5+} are observed. These peaks are consistent with the reported XPS spectra of Ce 3d and Mo 3d (Karthik et al., 2017).

3.2. Effect of various catalysts for AODS

In order to study the effect of catalyst structure in ADOS, oxidative desulfurization activity of different catalysts such as $Ce_2(MoO_4)_3$, $CeVO_4$, $Ce_2(WO_4)_3$ and Na_2MoO_4 were investigated under the same experimental conditions. As shown in Fig. 5, The MoO_4^{2-} has the highest sulfur removal in these catalysts owning the same cation. Efficiencies change follows the sequence $MoO_4^{2-} > VO_4^{3-} > WO_4^{2-}$. Similarly, based on the fact that the sulfur removal performance of $Ce_2(MoO_4)_3$ is much higher than that of Na_2MoO_4. It can conclude that Ce^{3+} also play a significant role in ODS. The above results indicate that the synergistic effect between Ce^{3+} and MoO_4^{2-} leads to higher sulfur removal.

3.3. Effect of reaction temperature

The reaction temperature is an important factor affecting the desulfurization rate. In AODS, the catalyst can show high sulfur removal at high temperature (>100°C). The oxidative desulfurization activity of $Ce_2(MoO_4)_3$ at different reaction temperatures was shown the Fig. 6, sulfur removal increases from 10.8% at 80°C to 99.6% at 100°C in 120 min. This is because increased the temperature can accelerate the collision rate between reactant molecules (Zhao et al., 2007). When the reaction temperature was increased from 100°C to 110°C, the sulfur removal rate increased to 99.6% in 80min. However, high temperature will also cause side reactions of hydrocarbons oxidation and the increase of energy consumption (Eseva et al., 2021). In conclusion, 100°C as the optimum reaction temperature.

3.4. Effect of catalyst dosage

The catalyst dosage is one of the most important parameters for the industrialization of ODS. The effect of $Ce_2(MoO_4)_3$ dosage on sulfur removal was investigated. The results are shown in Fig. 7, catalyst dosage increased from 0.02g to 0.05g results in the sulfur removal of DBT increasing from 58.8% to 99.6%. Nevertheless, the catalyst dosage was increased from 0.05g to 0.06g, the sulfur

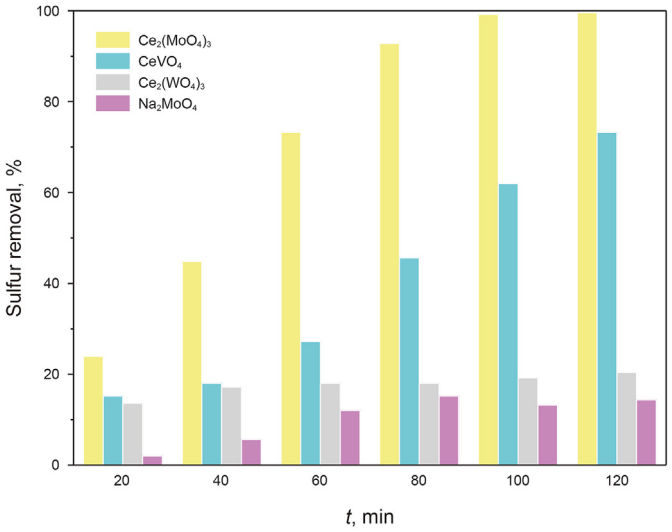

Fig. 5. Effect of different catalysts for sulfur removal (Reaction conditions: 20 mL model oil, O_2 airflow rate = 0.2L/min, T = 100°C, catalyst dosage = 0.05g).

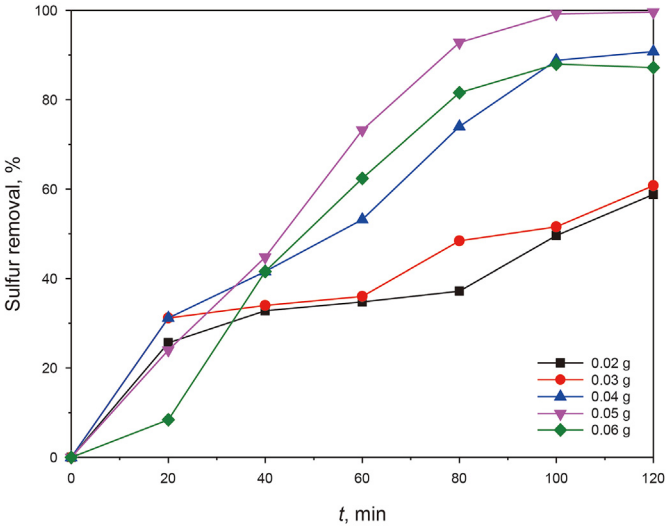

Fig. 7. Effect of the $Ce_2(MoO_4)_3$ dosage on sulfur removal (Reaction conditions: 20 mL model oil, O_2 airflow rate = 0.2L/min, T = 100°C).

removal decreased from 99.6% to 90.8%. The results show that increasing the amount of catalyst is beneficial to increasing the number of active sites (Qiu et al., 2016). However, excessive catalyst will cause agglomeration and limit the contact area with DBT, which will affect the diffusion of reactants and products, so reduce the sulfur removal (Eseva et al., 2021). Therefore, the optimal catalyst dosage of 0.05g was selected to oxidative desulfurization process.

3.5. Removal of different types of sulfide

In this experiment, the $Ce_2(MoO_4)_3$ has a high oxidation desulfurization activity on DBT in AODS. However, it is very necessary to study sulfur removal performance of catalysts for other sulfides such as BT and 4,6-DMDBT due to the diversity of sulfides in actual fuel. As shown in Fig. 8, the removal rate of 4,6-DMDBT and BT are 94% and 26%, they are lower than that of DBT. According to the literature (Zhao et al., 2017), the difference of

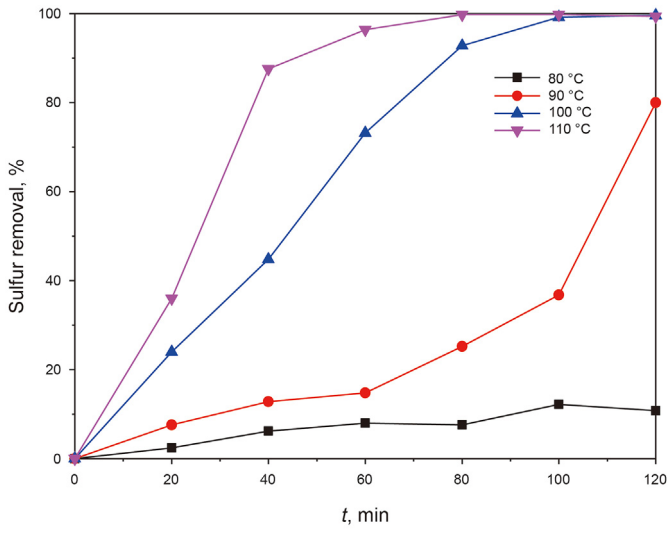

Fig. 6. Effect of reaction temperature on sulfur removal (Reaction conditions:20 mL model oil, O_2 airflow rate = 0.2L/min, $Ce_2(MoO_4)_3$ = 0.05g).

removal efficiency can be attributed to the electron cloud density of sulfur atoms and steric hindrance effect. The methyl groups in 4,6-DMDBT would hinder process of oxidative desulfurization reaction, resulting in a lower removal rate of DBT. The higher electron cloud density results the higher the oxidation desulfurization capacity. The electron densities of the S atom in DBT, 4,6-DMDBT and BT are 5.758, 5.760 and 5.739, respectively (Mao et al., 2017). Therefore, sulfur removal of DBT, 4,6-DMDBT and BT are affected by the steric hindrance and electron density (Otsuki et al., 2000).

3.6. Effects of olefins and aromatics

In ODS process, the presence of olefins and aromatics will affect the removal of organic sulfide. Here, toluene and cyclohexene are selected as the models of aromatics and olefins, effects of their addition on sulfur removal are explored in Fig. 9. Under optimal reaction conditions, when 5 wt%-toluene and 5 wt%-cyclohexene were added to 20 mL model oil, removal efficiency slightly decreased to 97.6% and 94.1%, respectively. It can be seen that both cyclohexene and toluene have a certain influence on the sulfur removal, which may be caused by the competitive reaction among toluene, cyclohexene and DBT (Liu et al., 2021). The results show that the sulfur removal of DBT in the AODS system is less affected by olefins and aromatics.

3.7. Recycling performance of $Ce_2(MoO_4)_3$

After the AODS reaction, the catalyst was filtered from the reaction system, and then washed with CCl_4 under a magnetic stirrer at 25°C for 30min. Finally, the catalyst was dried at 80 °C for 8 h. Thereafter, the recovered $Ce_2(MoO_4)_3$ catalyst was used in the next AODS under the optimal conditions. The exhibited results in Fig. 10 illustrates that the sulfur removal of DBT reduced to 94.7% after the five cycles. The recovered $Ce_2(MoO_4)_3$ catalyst was analyzed by FT-IR analysis measurement. The FT-IR spectrum was shown in Fig. 11. It can be seen that the fresh catalyst and the recovered catalyst have similar absorption peaks, Therefore, the catalyst has high stability.

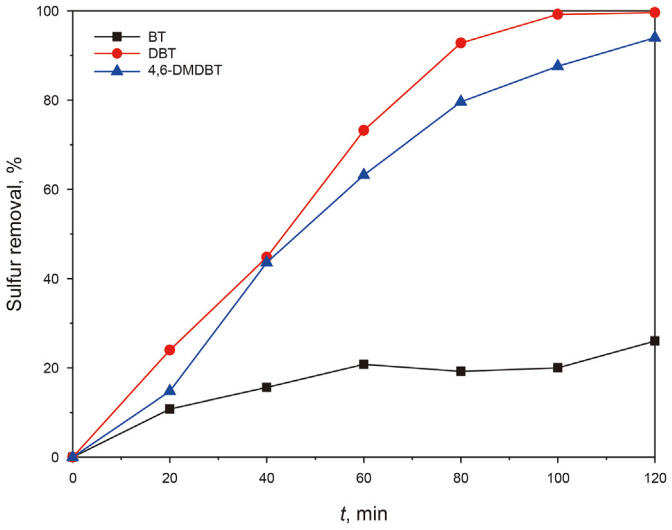

Fig. 8. Removal efficiency of different sulfides(Reaction conditions: 20 mL model oil, O_2 airflow rate = 0.2L/min, T = 100°C, $Ce_2(MoO_4)_3$ = 0.05g).

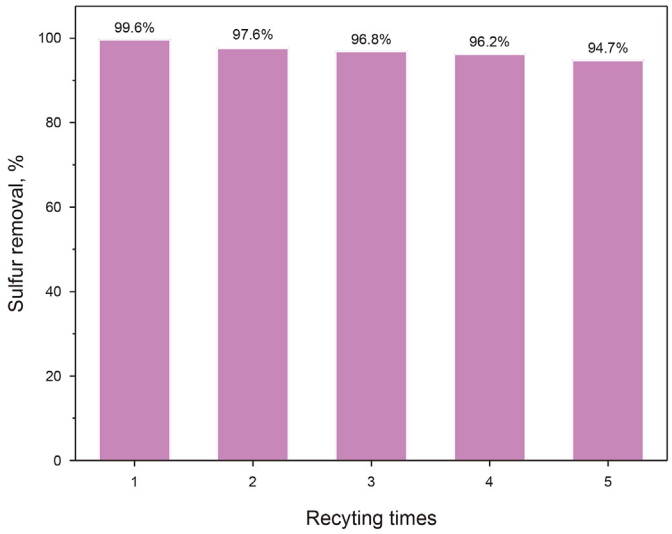

Fig. 10. Recycling performance of $Ce_2(MoO_4)_3$.

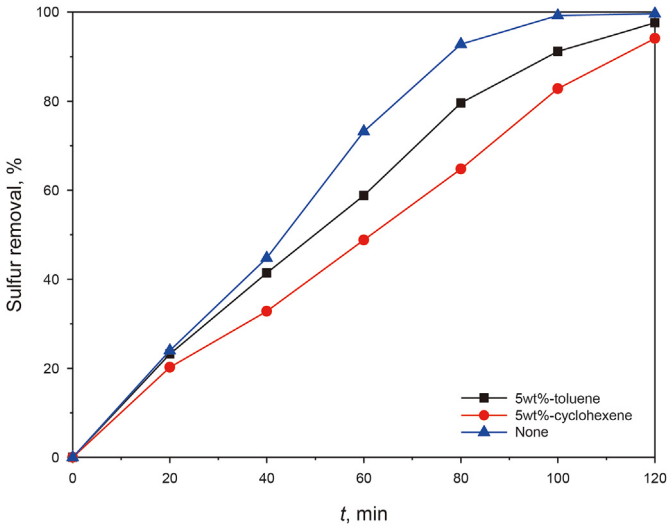

Fig. 9. Effect of olefins and aromatics on sulfur removal(Reaction conditions: 20 mL model oil, O_2 airflow rate = 0.2L/min, T = 100°C, $Ce_2(MoO_4)_3$ = 0.05g).

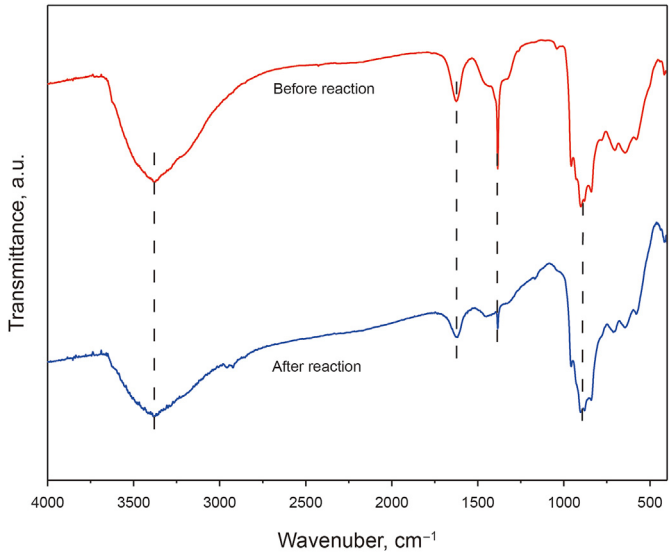

Fig. 11. FT-IR spectra of $Ce_2(MoO_4)_3$ before and after the reaction.

3.8. AODS mechanism in the presence of $Ce_2(MoO_4)_3$

In order to investigate aerobic oxidation desulfurization mechanism, a free radical capture experiment was designed. P-benzoquinone ($\cdot O_2^-$ trapping agents) and isopropanol ($\cdot$OH trapping agents) were added to AODS system, respectively. The experiment results are shown in Fig. 12. Sulfur removal after adding isopropanol can reach 97.2%, while the sulfur removal after adding p-benzoquinone is only 12%, this indicates that a large number of superoxide radicals [$\cdot O_2^-$] generated during the reaction are captured by p-benzoquinone, leads to reduce sulfur removal. The results show that [$\cdot O_2^-$] radical is the intermediate activated product of oxidation reaction.

After oxidative desulfurization reaction, The $Ce_2(MoO_4)_3$ was washed by CCl_4. The CCl_4 solution was evaporated by rotary evaporator to obtain oxidation products of the sulfur compounds, FT-IR characterization results of oxidation products are shown in Fig. 13(a). Two infrared absorption peaks at 1292 and 1166 cm^{-1}, which correspond to the characteristic absorption peaks of dibenzothiophene sulfone ($DBTO_2$). In addition, the obtained CCl_4 solution was analyzed by GC-MS measurement. The results are shown in Fig. 13 (b), the strong peak corresponding to $DBTO_2$ (m/z = 216.0) at 17.604 min was found. The FT-IR and GC-MS analysis proved that DBT was oxidized to $DBTO_2$.

In the research of aerobic oxidation of molybdenum-based catalysts (Lü et al., 2013; Ma et al., 2020; Xun et al., 2019), molybdenum sites have mixed valence states, the conversion between different valence states leads to the production of active molybdenum species. This experiment is different from these literatures. Through the XPS characterization, it can be seen that there is only Mo^{6+} in the $Ce_2(MoO_4)_3$ catalyst. Mo peroxides may be formed in the presence of oxygen. This phenomenon is very common in the oxidative desulfurization system with molybdenum-based catalyst (Jiang et al., 2019; Zhang et al., 2019). Refer to previous research (Shi et al., 2016, Zhang et al., 2019), the mechanism of oxidative desulfurization was shown in Fig. 14. First, oxygen molecules are

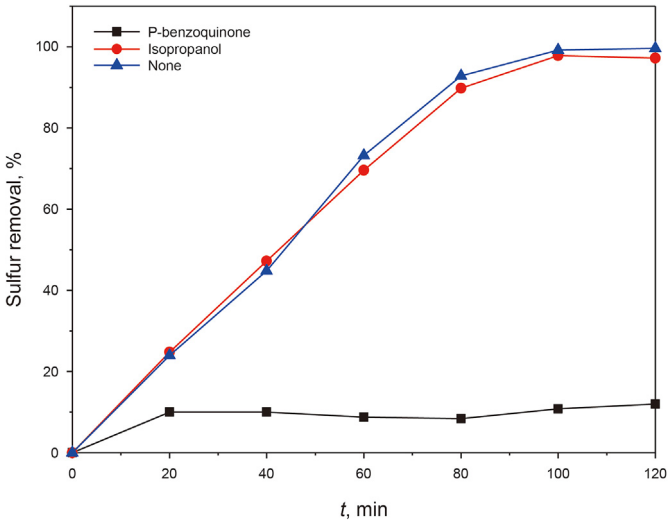

Fig. 12. Free radical capture experiment(Reaction conditions: 20 mL model oil, O_2 airflow rate = 0.2L/min, $T = 100°C$, $Ce_2(MoO_4)_3 = 0.05g$).

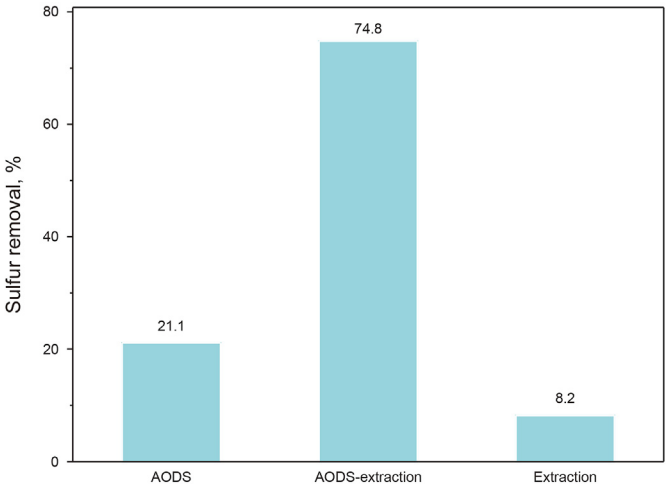

Fig. 15. AODS of diesel fuel.

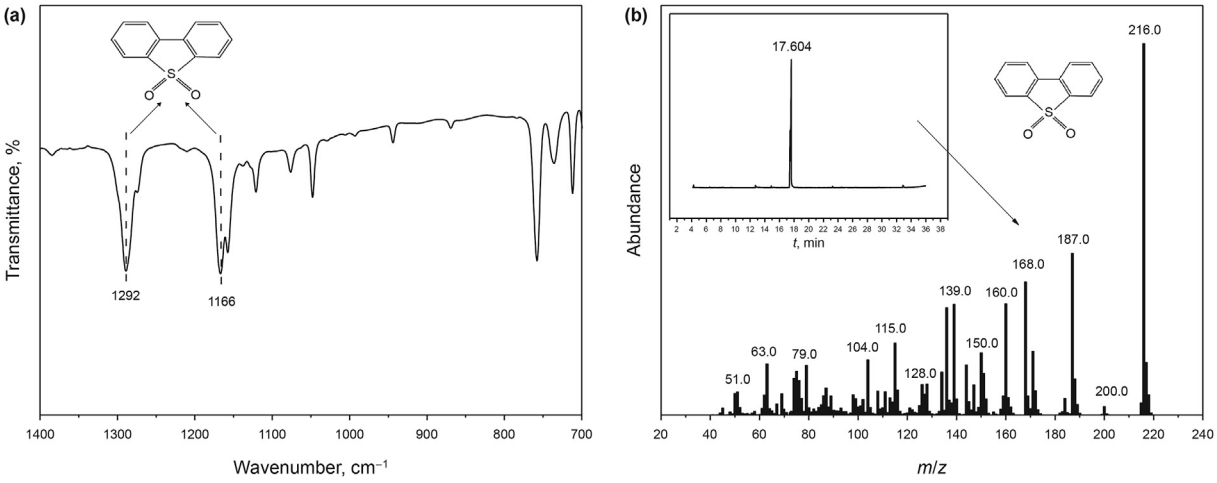

Fig. 13. **(a)** FT-IR spectrum and **(b)** GC-MS of oxidation products.

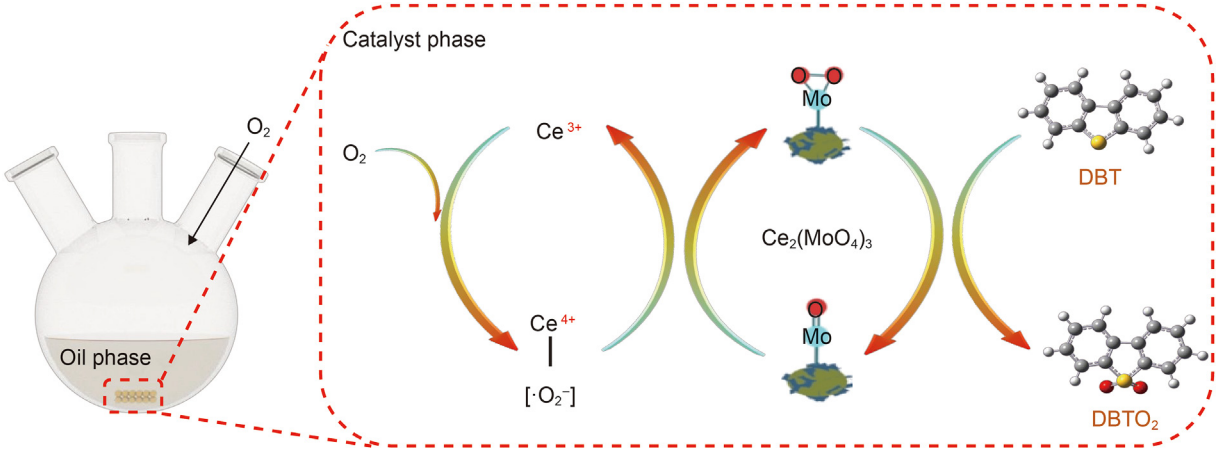

Fig. 14. AODS mechanism in the presence of $Ce_2(MoO_4)_3$.

adsorbed on the Ce^{3+} site of the catalyst to form Ce^{3+}-O_2, and some of the Ce^{3+}-O_2 further formation Ce^{4+}-[$\cdot O_2^-$] superoxide, then these Ce^{4+}-[$\cdot O_2^-$] interact with Mo sites on the catalyst to produce some active molybdenum species to further oxidize DBT compounds to $DBTO_2$ (Shi et al., 2016; Zhu et al., 2007).

3.9. AODS of diesel fuel

The aerobic desulfurization performance of $Ce_2(MoO_4)_3$ for diesel fuel with S-content of 150 μg/g was also investigated. It can be seen from Fig. 15, under optimal conditions, the sulfur removal of 21.1% was obtained. Compared with the model oil, the sulfur removal is too low due to the complexity of components in actual diesel. After the AODS, 1 mL of acetonitrile was added to the AODS system to extraction of oxidation products of sulfur, removal of sulfur compounds from diesel was reached 74.8%. When extraction desulfurization in diesel fuel was carried out by acetonitrile as extractant, sulfur removal is only 8.2%. The experimental results show that the AODS-extraction desulfurization system under the action of $Ce_2(MoO_4)_3$ can still remove most of the sulfide in diesel fuel.

4. Conclusions

$Ce_2(MoO_4)_3$ was synthesized by a simple reflux method using ammonium molybdate and cerium nitrate hexahydrate as raw materials. $Ce_2(MoO_4)_3$ was used as the catalyst in AODS systems. Sulfur removal of 99.6% for DBT, 94% for 4,6-DMDBT and 26% for BT were obtained under the optimized conditions of 20 mL model oil, catalyst dosage of 0.05g, oxygen flow rate of 0.2L/min, 100°C, respectively. The introduction of both olefin and aromatic hydrocarbon cannot significantly change the oxidative desulfurization activity of the catalyst. The superoxide radical generated by oxygen under the action of catalyst is the key factor for the oxidation of sulfide. The $Ce_2(MoO_4)_3$ has a strong regenerative capacity and the sulfur removal reached 94.7% after five cycles.

Acknowledgements

The authors also acknowledge the financial support of the Natural Science Foundation of Liaoning Province (2019-ZD-0064); Doctoral Fund of Liaoning Province (201501105).

References

Chi, M., Zhu, Z., Sun, L., et al., 2019. Construction of biomimetic catalysis system coupling polyoxometalates with deep eutectic solvents for selective aerobic oxidation desulfurization. Appl. Catal. B Environ. 259, 118089–118098. https://doi.org/10.1016/j.apcatb.2019.118089.

Dargahi, M., Masteri-Farahani, M., Shahsavarifar, S., et al., 2020. Microemulsion-mediated preparation of Ce_2 $(MoO_4)_3$ nanoparticles for photocatalytic degradation of crystal violet in aqueous solution. Environ. Sci. Pollut. Control Ser. 27 (11), 12047–12054. https://doi.org/10.1007/s11356-020-07816-2.

Dong, Y., Zhang, J., Ma, Z., et al., 2019. Preparation of Co–Mo–O ultrathin nanosheets with outstanding catalytic performance in aerobic oxidative desulfurization. Chem. Commun. 55 (93), 13995–13998. https://doi.org/10.1039/C9CC07452J.

Eseva, E., Akopyan, A., Schepina, A., et al., 2021. Deep aerobic oxidative desulfurization of model fuel by Anderson-type polyoxometalate catalysts. Catal. Commun. 149, 106256. https://doi.org/10.1016/j.catcom.2020.106256.

Jiang, W., Xiao, J., Dong, L., et al., 2019. Polyoxometalate-based poly (ionic liquid) as a precursor for superhydrophobic magnetic carbon composite catalysts toward aerobic oxidative desulfurization. ACS Sustain. Chem. Eng. 7 (18), 15755–15761. https://doi.org/10.1021/acssuschemeng.9b04026.

Kanai, S., Nagahara, I., Kita, Y., et al., 2017. A bifunctional cerium phosphate catalyst for chemoselective acetalization. Chem. Sci. 8 (4), 3146–3153. https://doi.org/10.1080/14328917.2015.1109173.

Karthik, R., Vinoth Kumar, J., Chen, S.-M., et al., 2017. A study of electrocatalytic and photocatalytic activity of cerium molybdate nanocubes decorated graphene oxide for the sensing and degradation of antibiotic drug chloramphenicol. ACS Appl. Mater. Interfaces 9 (7), 6547–6559. https://doi.org/10.1021/acsami.6b14242.

Kartsonakis, I.A., Kordas, G., 2010. Synthesis and characterization of cerium molybdate nanocontainers and their inhibitor complexes. J. Am. Ceram. Soc. 93 (1), 65–73. https://doi.org/10.1111/j.1551-2916.2009.03310.x.

Li, C., Li, D., Zou, S., et al., 2013. Extraction desulfurization process of fuels with ammonium-based deep eutectic solvents. Green Chem. 15 (10), 2793–2799. https://doi.org/10.1039/C3GC41067F.

Liu, X., Li, X., Zhao, R., et al., 2021. A facile Sol-gel method based on urea-$SnCl_2$ deep eutectic solvents toward synthesis of SnO_2/SiO_2 with high oxidation desulfurization activity. New J. Chem. 45, 15901–15911. https://doi.org/10.1039/D1NJ02526K.

Liu, Y., Han, L., Zhang, J., et al., 2020. Morphology-controlled construction and aerobic oxidative desulfurization of hierarchical hollow Co–Ni–Mo–O mixed metal-oxide nanotubes. Ind. Eng. Chem. Res. 59 (14), 6488–6496. https://doi.org/10.1021/acs.iecr.9b06988.

Lü, H., Ren, W., Liao, W., et al., 2013. Aerobic oxidative desulfurization of model diesel using a B-type Anderson catalyst $[(C_{18}H_{37})_2N(CH_3)_2]_3Co(OH)_6Mo_6O_{18}\cdot 3H_2O$. Appl. Catal. B Environ. 138, 79–83. https://doi.org/10.1016/j.apcatb.2013.02.034.

Luo, J., Wang, C., Liu, J., et al., 2021. High-performance adsorptive desulfurization by ternary hybrid boron carbon nitride aerogel. AIChE J., e17280 https://doi.org/10.1002/aic.17280.

Ma, Z., Zhang, J., Zhan, H., et al., 2020. Immobilization of Monodisperse Metal-Oxo-Cluster on Graphene for Aerobic Oxidative Desulfurization of Fuel, 140. Process Safety and Environmental Protection, pp. 26–33. https://doi.org/10.1016/j.psep.2020.04.041.

Mao, C-f, Zhao, R-x, Li, X-p, 2017. Propionic acid-based deep eutectic solvents: synthesis and ultra-deep oxidative desulfurization activity. RSC Adv. 7 (67), 42590–42596. https://doi.org/10.1039/C7RA05687G.

Nakagawa, Y., Tokuma, K., Nakaji, Y., et al., 2019. Aerobic oxidation of alkyl chain in alkylphenols over combination of Pt and Pd catalysts. Appl. Catal. Gen. 569, 149–156. https://doi.org/10.1016/j.apcata.2018.10.024.

Otsuki, S., Nonaka, T., Takashima, N., et al., 2000. Oxidative desulfurization of light gas oil and vacuum gas oil by oxidation and solvent extraction. Energy Fuels 14 (6), 1232–1239. https://doi.org/10.1021/ef000096i.

Qiu, L., Cheng, Y., Yang, C., et al., 2016. Oxidative desulfurization of dibenzothiophene using a catalyst of molybdenum supported on modified medicinal stone. RSC Adv. 6 (21), 17036–17045. https://doi.org/10.1039/C5RA23077B.

Sakthivel, T.S., Reid, D.L., Bhatta, U.M., et al., 2015. Engineering of nanoscale defect patterns in CeO_2 nanorods via ex situ and in situ annealing. Nanoscale 7 (12), 5169–5177. https://doi.org/10.1039/C4NR07308H.

Sampieri, A., Pronier, S., Blanchard, J., et al., 2005. Hydrodesulfurization of dibenzothiophene on MoS_2/MCM-41 and MoS_2/SBA-15 catalysts prepared by thermal spreading of MoO_3. Catal. Today 107, 537–544. https://doi.org/10.1016/j.cattod.2005.07.069.

Shi, Y., Liu, G., Zhang, B., et al., 2016. Oxidation of refractory sulfur compounds with molecular oxygen over a Ce–Mo–O catalyst. Green Chem. 18 (19), 5273–5279. https://doi.org/10.1039/C6GC01357K.

Tang, J., Cai, M., Xie, G., et al., 2020. Amino-induced 2D Cu-based metal–organic framework as an efficient heterogeneous catalyst for aerobic oxidation of olefins. Chem. Eur. J. 26 (19), 4333–4340. https://doi.org/10.1002/chem.201905249.

Wang, C., Chen, Z., Yao, X., et al., 2018. Decavanadates anchored into micropores of graphene-like boron nitride: efficient heterogeneous catalysts for aerobic oxidative desulfurization. Fuel 230, 104–112. https://doi.org/10.1016/j.fuel.2018.04.153.

Wang, C., Chen, Z., Yao, X., et al., 2017. One-pot extraction and aerobic oxidative desulfurization with highly dispersed V_2O_5/SBA-15 catalyst in ionic liquids. RSC Adv. 7 (62), 39383–39390. https://doi.org/10.1039/C7RA07286D.

Wang, C., Jiang, W., Chen, H., et al., 2021. Pt nanoparticles encapsulated on V_2O_5 nanosheets carriers as efficient catalysts for promoted aerobic oxidative desulfurization performance. Chin. J. Catal. 42 (4), 557–562. https://doi.org/10.1016/S1872-2067(20)63685-3.

Wang, C., Li, H., Zhang, X., et al., 2020. Atomic-Layered α-V_2O_5 nanosheets obtained via fast gas-driven exfoliation for superior aerobic oxidative desulfurization. Energy Fuels 34 (2), 2612–2616. https://doi.org/10.1021/acs.energyfuels.9b04401.

Wu, P., Wu, Y., Chen, L., et al., 2020. Boosting aerobic oxidative desulfurization performance in fuel oil via strong metal-edge interactions between Pt and h-BN. Chem. Eng. J. **380** 122526. https://doi.org/10.1016/j.cej.2019.122526.

Xing, G., Guo, H., Yang, Z., et al., 2016. Controllable synthesis and photocatalytic properties of spherical and flower-like $Ce_2(MoO_4)_3$ hierarchical architectures. Mater. Res. Innovat. 20 (4), 272–279. https://doi.org/10.1080/14328917.2015.1109173.

Xun, S., Jiang, W., Guo, T., et al., 2019. Magnetic mesoporous nanospheres supported phosphomolybdate-based ionic liquid for aerobic oxidative desulfurization of fuel. J. Colloid Interface Sci. 534, 239–247. https://doi.org/10.1016/j.jcis.2018.08.115.

Yousefi, T., Khanchi, A.R., Ahmadi, S.J., et al., 2012. Cerium (III) molybdate nanoparticles: synthesis, characterization and radionuclides adsorption studies. J. Hazard Mater. 215, 266–271. https://doi.org/10.1016/j.jhazmat.2012.02.064.

Zhang, Q., Zhang, J., Yang, H., et al., 2019. Efficient aerobic oxidative desulfurization over Co–Mo–O bimetallic oxide catalysts. Catal. Sci. Technol. 9 (11), 2915–2922. https://doi.org/10.1039/C9CY00459A.

Zhao, D., Wang, J., Zhou, E., 2007. Oxidative desulfurization of diesel fuel using a

Brønsted acid room temperature ionic liquid in the presence of H_2O_2. Green Chem. 9 (11), 1219–1222. https://doi.org/10.1039/B706574D.
Zhao, R., Li, X., Su, J., et al., 2017. Preparation of WO_3/g-C_3N_4 composites and their application in oxidative desulfurization. Appl. Surf. Sci. 392, 810–816. https://doi.org/10.1016/j.apsusc.2016.08.120.
Zhen, Y., Wang, J., Fu, F., et al., 2019. The novel z-scheme ternary-component Ag/AgI/α-MoO_3 catalyst with excellent visible-light photocatalytic oxidative desulfurization performance for model fuel. Nanomaterials 9 (7), 1054. https://doi.org/10.3390/nano9071054.
Zhu, W., Li, H., Jiang, X., et al., 2007. Oxidative desulfurization of fuels catalyzed by peroxotungsten and peroxomolybdenum complexes in ionic liquids. Energy Fuels 21 (5), 2514–2516. https://doi.org/10.1021/ef700310r.